T41D-0650, Dec. 14, 2017, AGU Fall Meeting

Shiro HIRANO (s-hrn@fc.ritsumei.ac.jp, Ritsumeikan Univ., Japan)

Mathematical modeling and numerical simulation of unilateral dynamic rupture propagation along very-long reverse faults

Acknowledgment

Data: trench by Bird [2003 G^3]; fault by Burton & Hall [2014 *GRL*]; event catalogs by USGS and GCMT; plate motion based on GSRM v2.1 by UNAVCO. This work was supported by JSPS KAKENHI Grant No. 17H02857. I am grateful to Takehito Suzuki and Ryo Okuwaki for helpful discussions on section 3 and 4, respectively.

1. Introduction

Unilateral rupture propagation along reverse faults:

- 2004 Sumatra, Indonesia(Mw9.1) [Ishii *et al.*, 2005 *Nature*]
- 2008 Wencuan, China(Mw8.0) [Xu *et al.*, 2009 G^3]
- 2010 Maule, Chile(Mw8.8) [Pulido *et al.*, 2011 *EPSL*]

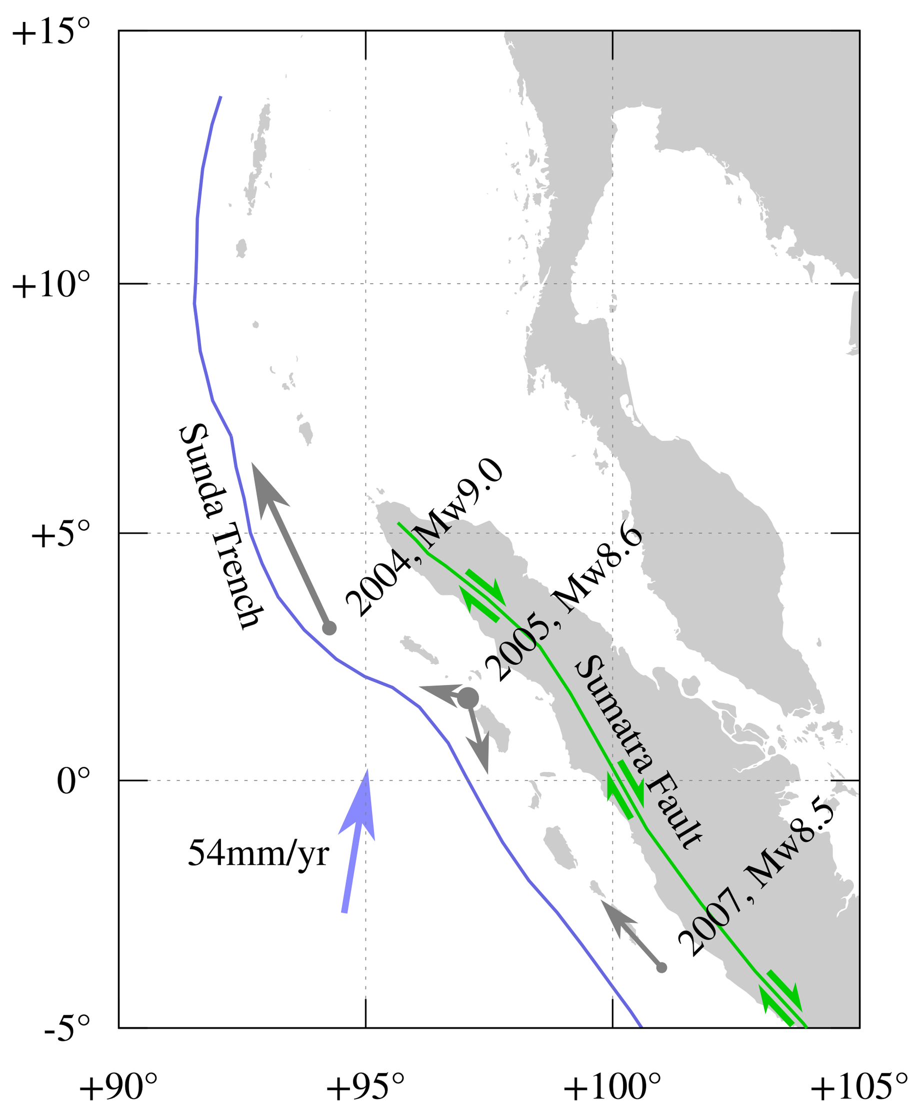

Fig.1. Plate motion (blue arrow), fault slip (green arrows) and rupture directions (gray arrows) around the Sunda trench.

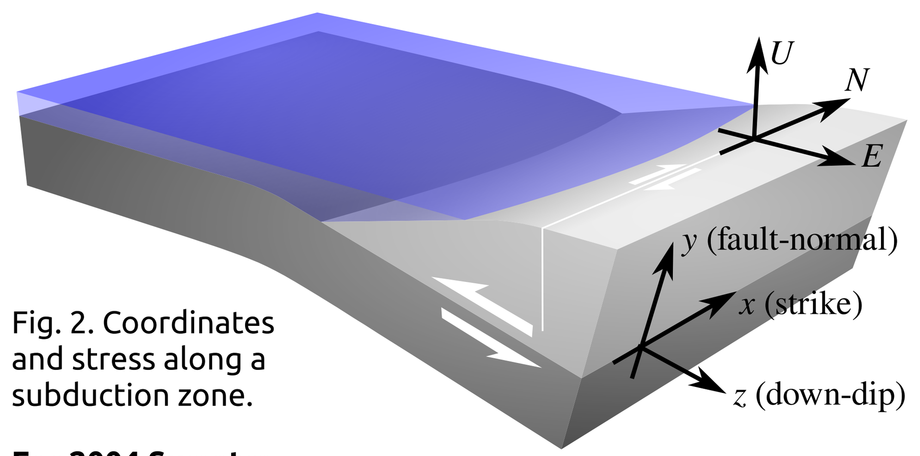

Fig. 2. Coordinates and stress along a subduction zone.

For 2004 Sumatra

unbreakable barrier or no strain energy in the south?

... Maybe NO! (∵ Mw8.6 event just after three months)

Known properties [McGuire *et al.*, 2002 *BSSA*]

- *"Approximately 80% of large shallow ruptures are predominantly unilateral"*
- *"A uniform distribution of epicenters along the fault leads to a predominance of unilateral rupture for this(= 1-D uniform slip fault) model"*

Motivation

Deterministic mechanism?

Relevant to **tectonic settings?**

Simple model?

Generality in observations?

2. Mathematical Modeling

2.1. Tectonic settings

Oblique subduction and/or inland strike-slip fault systems

(Thrust + Strike-slip) fault compatible stress tensor = oblique background shear stress in x-y plane (i.e., $\psi > 0$)

Bimaterial system w.r.t. the rigidity μ, density ρ, and S-wave speed β

μ^+, ρ^+, and β^+ are smaller than μ^-, ρ^-, and β^-, respectively ($\pm$: sign of y)

Mode-III rupture propagation dominates

A bimaterial effect contributes to unilateral rupture for **mode-II** (e.g., Weertman, 1980 *JGR*; Hirano & Yamashita, 2016 *BSSA* for theory, Andrews & Ben-Zion 1997 *JGR*; Cochard & Rice 2000 *JGR*; DeDontney *et al.*, 2011 *JGR* for numerical simulation, and Rubin & Gillard, 2000 *JGR*; Zaliapin & Ben-Zion, 2011 *GJI* for observation).

How does it work for mode-III?

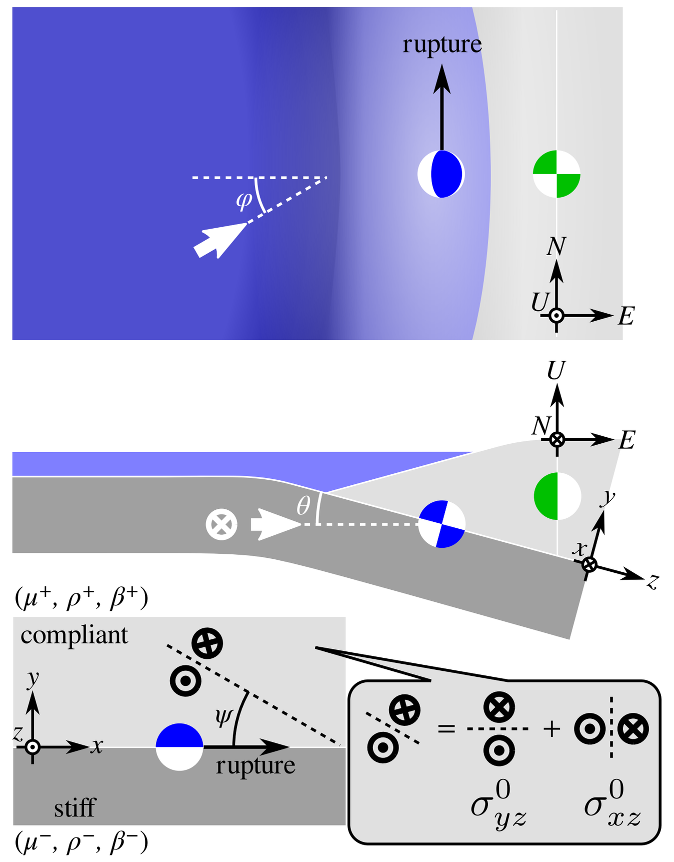

Fig. 3. Tectonic setting and parameters.

2.2. Steady-state mode-III pulse-like rupture

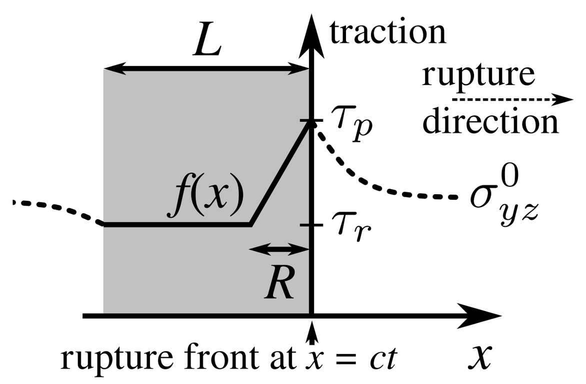

Fig. 4. Traction distribution given in the pulse ($f(x)$:solid) and to be obtained (dotted) for the model.

friction = initial stress + stress perturbation due to slip

$$f(x) = \sigma^0_{yz} + \frac{\mu}{c}\sqrt{1-(c/\beta)^2}\int_{ct-L}^{ct}\frac{[v](\xi)}{\xi - x}\frac{d\xi}{\pi}.$$

Limited and constant length, L, of currently-slipping region propagating with a constant speed c.

shear traction varies from its peak τ_p at the front to the dynamic friction level τ_r continuously within distance R.

Off-fault elastic stress perturbation and total stress can be obtained analytically [Muskhelishvili, 1953; Rice *et al.*, 2005 *BSSA*].

Applicable to a bimaterial and obliquely stressed system.

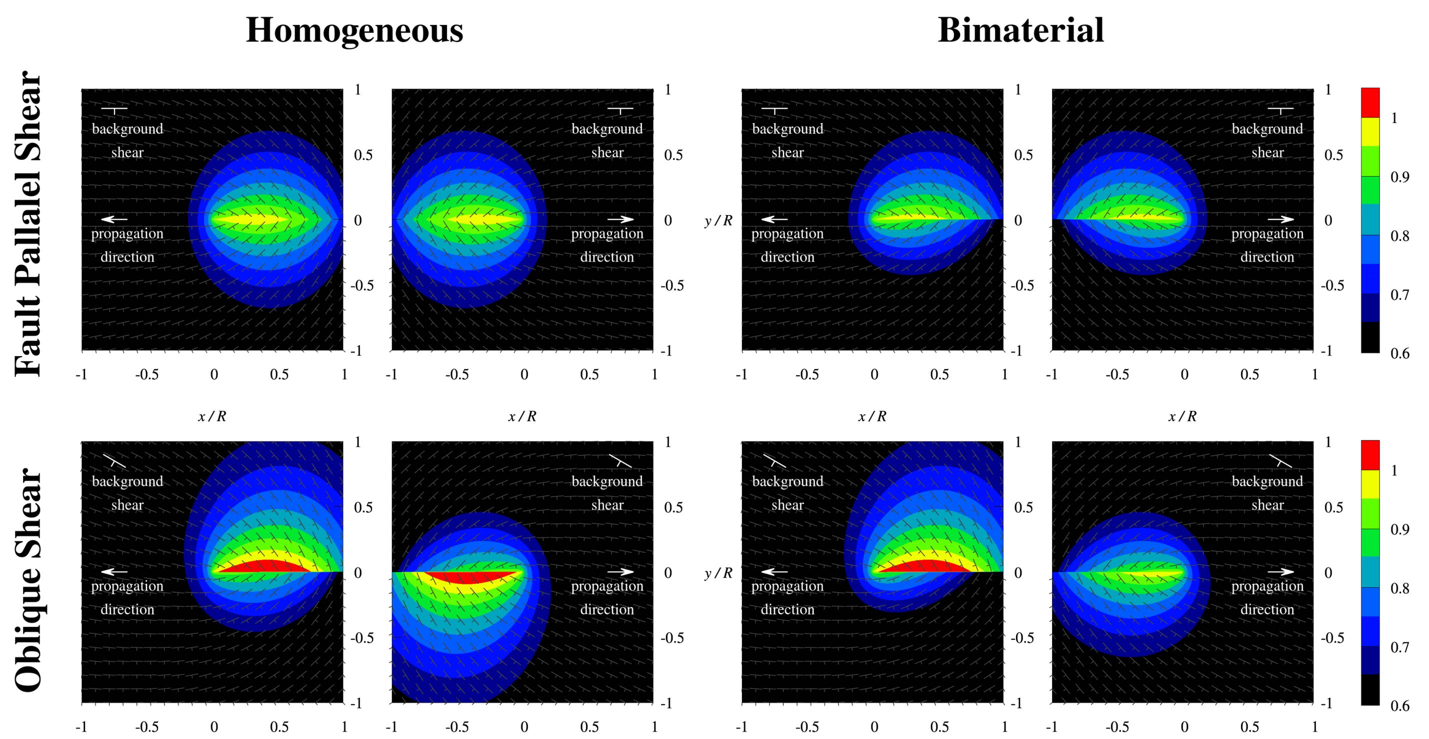

Fig. 5. Off-fault total stress normalized by strength of the medium. The upper left is the same as that of Rice *et al.*, [2005 *BSSA*], while others are done by this study.

Speculation from the mathematical (linear elastic) model

Stress intensity ⇒ damage ⇒ energy dissipation ⇒ prevention of rupture acceleration ⇒ **rightward unilateral rupture propagation**

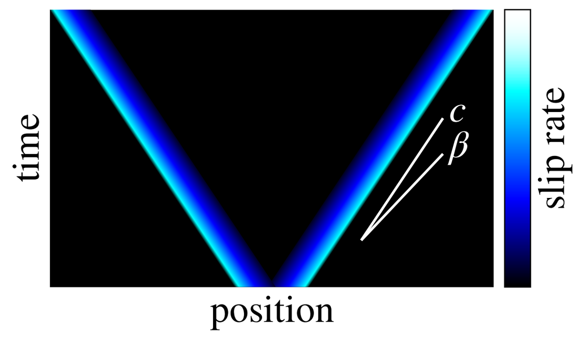

Fig. 6. Schematic illustration of steady-state pulse-like rupture.

2.3. Interpretation

Galilean transformation $x \pm ct \mapsto x \; (\partial_t \mapsto \pm c\partial_x)$

$$\partial_t^2 u = \left(\beta^\pm\right)^2 \Delta u \mapsto \partial_x^2 u + \left(\gamma^\pm\right)^2 \partial_y^2 u = 0,$$

where $\gamma^\pm := \frac{1}{\sqrt{1-\left(c/\beta^\pm\right)^2}}$ is the material-dependent Lorentz factor that describes expansion of stress intensity along y-direction as rupture accelerates.

3. Finite-Difference simulation for spontaneous rupture

Table 1. Parameters for section 2 and 3.

quantity	section 2	section 3.
ψ	0° or 30°	30°
μ^-/μ^+	1 or 2	2
ρ^-/ρ^+	1	1
τ_{th}/τ_p	1.05	1.02
R/L	0.001	N/A
$S = \frac{\tau_p - \sigma^0_{yz}}{\sigma^0_{yz} - \tau_r}$	depends on R/L	$1.25 - 2.0$
τ_r/τ_p	0.2	$0.64 - 0.57$
c/β^+	0.7	variable
c_a/β^+	N/A	0.1
T	$= R/c$	0.5

3.1. Off-fault damage modeling strategies

✗ Strain threshold model [Lyakhovski *et al.*, 1997 *JGR*] or microcrack-density dependent model [Suzuki, 2012 *JGR*]

Strain increment is related to damage variable (i.e., **independent of background stress**).

✓ Stress threshold model [Andrews, 1976 *JGR*; 2005 *JGR*; Templeton & Rice, 2008 *JGR*; Dunham *et al.*, 2011 *BSSA*]

Inelastic response when **total stress exceeds some threshold** τ_{th}

modeled as **the Drucker-Prager viscoplasticity** (∼ the Mohr-Coulomb yield criterion [Templeton & Rice, 2008 *JGR*]) with **rate dependence** [Dunham *et al.*, 2011 *BSSA*].

$$\rho\partial_t v = \nabla\cdot\sigma,$$
$$\partial_t\sigma = \partial_t\sigma^* - \mu\max\left(0, \frac{\|\sigma^*\|-\tau_{th}}{\eta}\right)\frac{\sigma^*}{\|\sigma^*\|},$$
$$\partial_t\sigma^* := \mu\nabla v,$$

and $v = 0, \sigma = \sigma^* = \left(\sigma^0_{xz}, \sigma^0_{yz}\right)^T$ for $t = 0$.

Plastic strain rate is $\partial_t\epsilon^P = \frac{1}{\mu}\,\partial_t\left(\sigma^* - \sigma\right)$.

3.2. On-fault conditions

Artificial nucleation

Spreading bilaterally with speed $c_a = 0.1\beta^+$ from the origin.

Fracture criterion and friction

Slip is allowed after $\sigma_{yz} = \sigma^0_{yz} + \delta\sigma_{yz} \geq \tau_p$ is satisfied or an edge of the nucleation zone arrives.

A time-weakening friction from $\sigma_{yz} = \tau_p$ to τ_r [Andrews, 2005 *JGR*] with time T.

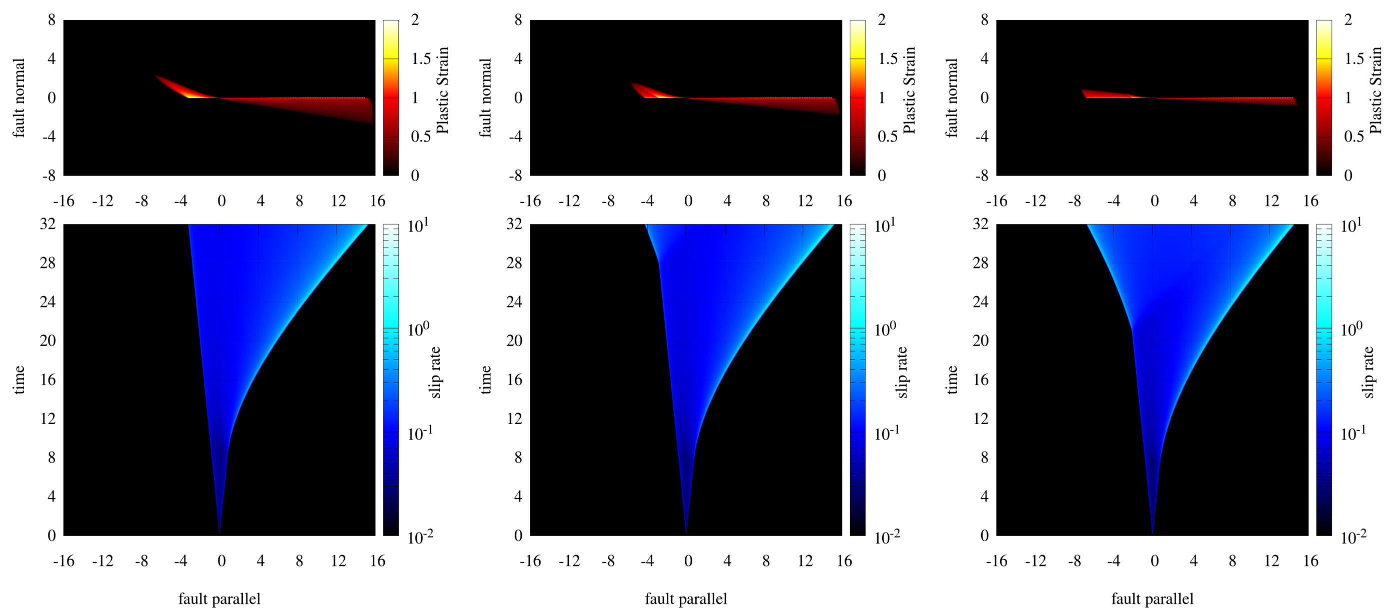

Fig. 7. Off-fault plastic strain (red) and on-fault slip velocity history (blue) for $S = 1.25$ (left), 1.5 (center), and 2.0 (right).

Results from the numerical (inelastic) model

As expected for smaller S.

Effective critical crack length is strongly asymmetric.

Delayed rupture towards the opposite direction may occur for larger S.

4. Discussion & Conclusions

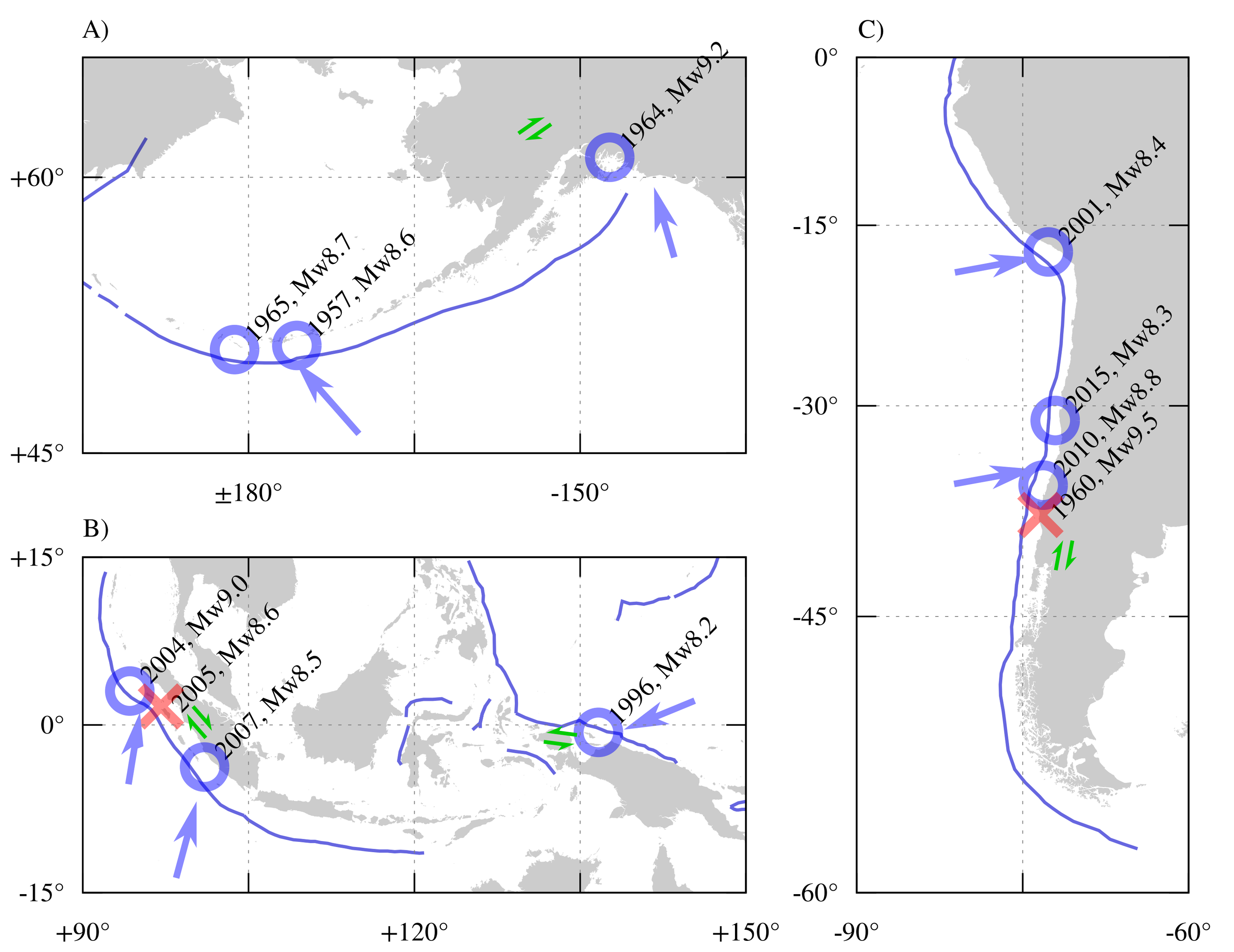

- For megathrust regions, the model suggests that preffered rupture direction coincides with trench-parallel component of the subducting plate motion and/or motion of continental plate's edge along strike-slip faults.
- At least 8 of 11 megathrust events of Mw $\geq$ 8.2 with oblique subduction obey the speculation by the model.
- Anti-preferred rupture events are not minority for Mw $<$ 8.2 (e.g., 1944 Tonankai, Japan (Mw8.1?); 1995 Antofagasta, Chile (Mw8.0); 2015 Iquique, Chile (Mw8.1).). Not long enough?
- Even an inland reverse fault, the 2008 Wenchuan, China (Mw8.0), event could be interpreted (∵ the footwall is compliant sediment and the hanging wall is stiff mountain; EW compression and NE rupture with NW dipping).
- No sufficiently large and modern events in Nankai Trough, Japan, but possibly westward therein.

Fig. 8. preferred (Blue circles) and anti-preferred (red crosses) rupture directions, and plate motions for Aleutian-Alaska(A), Indonesia(B), and Peru-Chile(C) regions.

Table 1. Consistency of rupture direction and plate motion on three megathrust regions shown in Fig. 8. All of Mw $\geq$ 8.2 events are extracted from USGS (1950-1975) and GCMT (1976-) catalogs for the regions.

Consistency	Year	Location	Mw	Plate Motion	Rupture Direction	Interpretation & evidences	References
✔	1957	Aleutian (A)	8.6	NNW	W	Tsunami inversion suggested dominant moment release in west, while the epicenter is almost midpoint of aftershock distribution.	Johnson *et al.*, 1994 *PAGEOPH*
✘	1960	Valdivia (C)	9.5	ENE	S	The epicenter is located on the north edge of aftershock distribution.	Fujii & Satake, 2013 *PAGEOPH*
✔	1964	Southern Alaska (A)	9.2	NNW	WSW	No obvious oblique subduction, but the Denali fault, matured right-lateral strike-slip fault, in north	Doser & Brown, 2001 *BSSA*; Mavroeidis *et al.*, 2008 *BSSA*; Koons *et al.*, 2010 Tectonics
✔	1965	Aleutian (A)	8.7	NNW	W	The epicenter is located on the east edge of aftershock distribution.	Beck & Christensen, 1991 *PAGEOPH*
✔	1996	Biak (B)	8.2	WSW	W→E	Westward rupture 30 seconds preceded eastward one.	Henry & Das, 2002 *JGR*
✔	2001	Southern Peru (C)	8.4	ENE	SE	By geodetic inversion.	Giovanni *et al.*, 2002 *GRL*
✔	2004	Sumatra-Andaman (B)	9.0	NNE	NNW	By back projection, teleseicmic inversion, and many other studies.	Ishii *et al.*, 2005 *Nature*; Briggs *et al.*, 2006 *Science*
✘	2005	Sumatra (B)	8.6	NNE	NW&SE	Bilateral rupture accompanied by two slip patches in north and south of the epicenter	Konca *et al.*, 2006 *BSSA*; Briggs *et al.*, 2006 *Science*
✔	2007	Southern Sumatra (B)	8.5	NNE	NW	By Tsunami/InSAR inversions	Lorito *et al.*, 2008 *GRL*; Fujii & Satake, 2008 *EPS*; Gusman *et al.*, 2010 *JGR*
✔	2010	Maule (C)	8.8	ENE	N	By teleseismic inversion and hybrid back projection	Pulido *et al.*, 2011 *EPS*; Okuwaki *et al.*, 2014 *Sci. Rep.*
✔?	2015	Illapel (C)	8.3	ENE	NE→NW	Non-negligible along-dip (EW) migration while the northward along-strike rupture is consistent with the theory	An *et al.*, 2015 *BSSA*

PDF poster and reference list are available at
http://interfacial.jp/
Click "Presentations" to jump to download link